Industrial Engineering Journal
ISSN: 0970-2555
Volume : 51, Issue 04, April : 2022

Density functional theory modelling of polarons: TiO2 as a case study

Monalisha Panda
Assistant Professor, Department of Basic Science and Humanities , Nalanda Institute of Technology, Bhubaneswar, Odisha, India
e-mail-monalishapanda@thenalanda.com

Abstract
Today, one of the most popular and effective methods for examining the characteristics of polarons and their effects on materials is density functional theory (DFT). Here, we thoroughly examine the elements of theoretical calculations that are essential for producing predictions that are consistent with experimental findings. We examine the production of polarons on the (110) surface and subsurface atomic layers of rutile TiO2, a prototype polaronic molecule. As anticipated, the parameter U utilised in the DFT + U formalism to correct the electronic correlation has an impact on the charge localization, local structural distortions, and electronic characteristics of polarons. Additionally, strain can cause the polaron localization to shift to other locations; for example, surface and subsurface polarons respond differently to distinct local environments.

Keywords: surface science, polarons, DFT, catalysis

1. Introduction

Excess charge in polarizable materials can couple to the lattice phonons and form polaron quasiparticles [1]. Since their formulation in the early twentieth century [2–5], polarons have extensively been studied in physics, materials science and chemistry [6–10], and continue nowadays to be of large interest due also to their impact on a wide range of modern technologies [11–16]. Titanium dioxide is a prototypical example for the study of polarons in materials [16–21]. In its rutile form, TiO_2 is likely to host so-called small electron polarons, i.e., electrons strongly localized on one or few lattice sites, and associated to evident distortions of the local structure [22, 23]. The long series of diverse experiments performed on this compound [1, 21] has been accompanied by analysis at the density-functional theory (DFT) level, which is a broadly used technique for investigations of polaronic properties [24–39]. Modelization of the localized electrons requires a correction of the electronic correlation of the Ti *d* orbitals, that can be efficiently achieved by adopting the DFT + *U* technique: an additional energy term is introduced in the Hamiltonian, and tuned by a parameter *U* [40]. The value of *U* is typically determined by comparing the electronic properties of the simulated system with the experimental measurements, or by relying on different *ab initio* approaches [41–46].

Figure 1 collects general aspects of polaron formation on the rutile TiO_2(110) surface as obtained by DFT + *U* calculations. Oxygen vacancies (V_O) that easily develop on the surface of rutile samples introduce excess electrons into the system. Assuming a rigid band model, one would expect this excess charge to fill the bottom of the conduction band, with a transition from a semiconducting density of states (DOS),

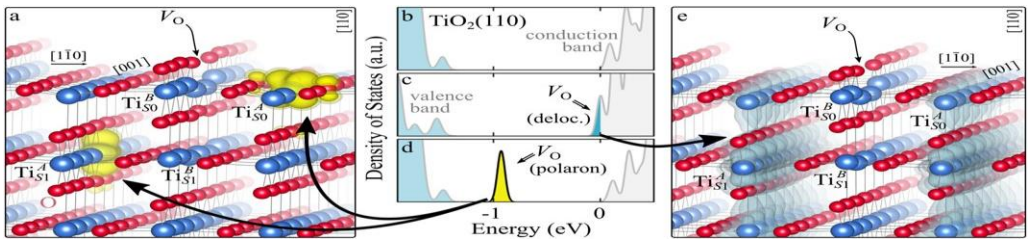

Figure 1. Excess electrons on rutile TiO_2(110). DOS for a pristine slab (b), and a slab with one V_O (oxygen vacancy concentration c_{V_O} = 5.6%) in the delocalized (c) and polaronic (d) solutions. Panels a and e show the spatial distribution of the charge density corresponding to the polaronic in-gap peak and to the electrons at the bottom of the conduction band, respectively (yellow and gray colors correspond to high and low isosurface levels).

Industrial Engineering Journal
ISSN: 0970-2555
Volume : 51, Issue 04, April : 2022

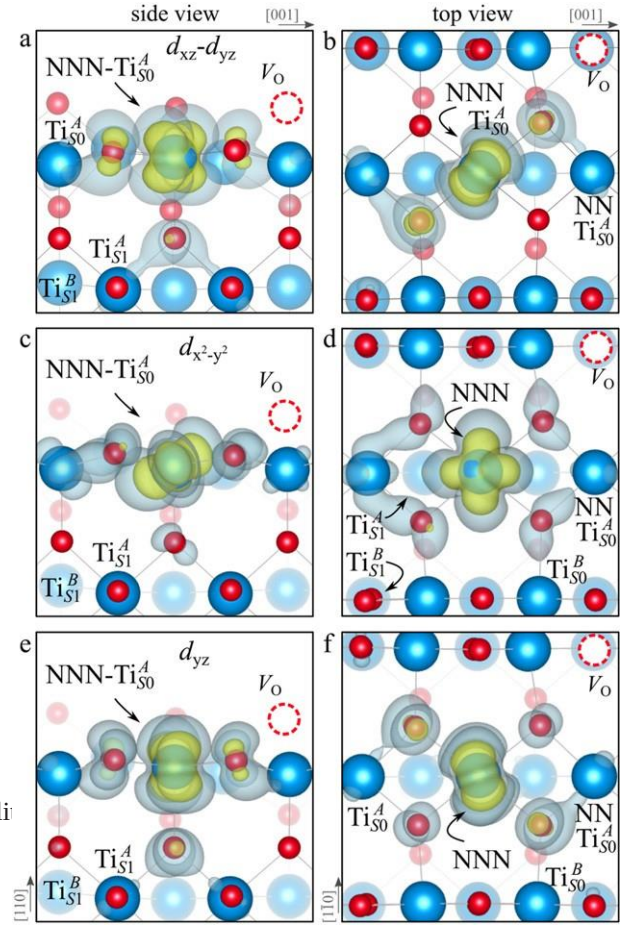

Figure 2. The NNN – Ti^A_{S0} polaron. Side (a), (c) and (e) and top (b), (d) and (f) views for three different orbital symmetries obtained for the NNN – Ti^A_{S0} polaron: d_{xz}–d_{yz} (a) and (b), $d_{x^2-y^2}$ (c) and (d) and d_{yz} (e) and (f). Yellow and gray colors represent high and low isosurface levels for the polaronic charge density, respectively.

bili

typical of the pristine surface (figure 1(b)), to a metallic phase (figure 1(c)): we refer to this system as delocalized solution, since the electronic states are spatially dispersed throughout the material (figure 1(e)). Formation of a polaronic state with the excess charge localized at single Ti atoms and associated to a sharp state in the energy gap (figures 1(a) and (d)) is predicted by DFT + *U* as a more stable solution. The charge localization can occur at different lattice sites, leading to polarons characterized by different properties and stability: usually, the most suitable hosting sites are the subsurface Ti atoms lying below the five-fold coordinated atoms (Ti^A_{S1}, see labeling in figure 1) [47–50]. However, environmental conditions and/or computational details can alter the polaron stability, and favor the charge localization elsewhere, especially on the surface Ti^A_{S0} atoms [26, 27, 43, 44, 51–55].

Here, we systematically analyze the polaronic properties of rutile TiO_2(110), and the dependence on physical quantities, such as lattice strain, and the correction *U* of the electronic correlation in DFT + *U* calculations. In particular, we describe the change in the charge localization, local structural distortions and electronic properties of polarons as determined by different values of the *U* parameter. Moreover, we show that the application of strain along the [001] direction can reverse the stability of Ti^A_{S1} and Ti^A_{S0} polarons, in agreement with experimental observations, due to their different orbital symmetries and different interaction with the surrounding local structure. We emphasize that a precise knowledge of the effects of the parameters used in DFT calculations is key to obtain reliable predictions, in agreement with experiments: we conclude the manuscript by showing the effects of the altered relative sta- $_{S1}$ and Ti^A_{S0} polarons on a well studied application, the adsorption of CO molecules on the rutile surface [56].

2. Methods

This study was conducted in the framework of density functional theory (DFT), by using the Vienna *ab initio* simulation package (VASP) [57–59]. We adopted the generalized gradient approximation (GGA) with the Perdew, Burke, and Ernzerhof parametrization [60], optimized to account for Van-der-Waals dispersion interactions as originally proposed by Dion *et al*. (optPBE) [61, 62] in order to properly model the interaction with adsorbates. A correction for the electronic correlation was included by using an on-site effective *U* [40] of U^{cRPA} = 3.9 eV on the *d* orbitals of the Ti atoms [63] (optPBE +*U*

Industrial Engineering Journal
ISSN: 0970-2555
Volume : 51, Issue 04, April : 2022

calculations), previously determined by constrained random-phase approximation (cRPA) calculations in bulk rutile [35]. The rutile surfaces were modeled with asymmetric slabs containing five Ti layers in large two-dimensional 9 × 2 and 6 × 2 unit cells, using low-temperature experimental lattice parameters [21], with the inclusion of a vacuum region of 15 Å. In our reference frame, the *x*, *y* and *z* Cartesian axis correspond to the [001], [1$\bar{1}$0] and [110] crystallographic directions, respectively. All atomic sites except atoms on the bottom two layers were relaxed using standard convergence criteria with a plane-wave energy cutoff of 400 eV, and using the Γ point for sampling the reciprocal space.

Oxygen vacancies (V_O) were included by removing one two-fold coordinated surface O atom from the 9 × 2 slabs, and one or two O atoms from the 6 × 2 slabs, corresponding to concentrations of c_{V_O} = 5.6%, 8.3%, and 16.7%, respectively. Every V_O supplies two excess electrons, eligible to form two polarons [35]. We used VESTA [64] to show the spatial extension of the excess charge. The polaron formation energy E_{POL} (Ti^A_{S1}) for sub-surface Ti^A_{S1} polarons distributed in equivalent localization sites in the slab is defined as the energy difference between the free energy of the system hosting polarons (E_{loc}) as compared to the energy of the system with the excess charge delocalized (E_{del}), divided by the number *n* of polarons in the slab: $E_{POL} = (E_{loc} - E_{del})/n$. Single surface Ti^A_{S0} polarons were modeled by replacing one of the sub-surface Ti^A_{S1} polarons in the slab: the polaron formanergy E_{POL} (Ti^A_{S0}) was calculated by further subtracting the E_{POL} (Ti^A_{S1}) of the n_{S1} sub-surface polarons, E_{POL} (Ti^A_{S0}) tion The results for E_{POL} (Ti^A_{S1}) are comparable to the values obtained by modeling one single Ti^A_{S0} polaron and removing all remaining excess electron from the system, with the addition of a compensating background charge (results obtained in this setup are not shown here) [65]. The convergence of E_{POL} for the various polarons with respect to the modeling setup (number of atomic layers and lateral size of the slab) was discussed in previous works [65]. The CO adsorption energy (E_{ads}) is calculated by subtracting from the energy E^{CO}_i of the system with the CO molecule adsorbing in a specific configuration *i*, the energy E_{S1} of the clean slab hosting two Ti^A_{S1} polarons in their optimal configuration and the energy E^{CO}_{gas} of the CO molecule in the gas phase [54]: $E_{ads} = E^{CO}_i - E_{S1} - E^{CO}_{gas}$

3. Results and discussion

Oxygen vacancies on the TiO_2(110) surface cause the formation of polarons, as described in the Introduction and shown in figure 1. Typically, sub-surface Ti^A_{S1} ions are the most favorable sites for polaron localization, and they have been described in detail in the literature [16–21, 27–29, 35, 47–50, 52–55]. These Ti^A_{S1} polarons show a d_{z^2}–$d_{x^2-y^2}$ orbital symmetry, with

Table 1. The NNN − Ti^A polaron. Orbital characters and relative energy stability (ΔE) for the three different NNN − Ti^A_{S0} polarons (d_{xz}–d_{yz}, $d_{x^2-y^2}$ and d_{yz}).

NNN − Ti^A_{S0}	ΔE	d_{xy}	d_{xz}	d_{yz}	$d_{x^2-y^2}$	d_{z^2}
d_{xz}–d_{yz}	0	—	**24**	**41**	—	—
$d_{x^2-y^2}$	+25	—	10	1	**50**	3
d_{yz}	+40	—	6	**58**	—	—

table 1 report the different solutions as obtained for a polaron on the next nearest neighbor NNN − Ti^A_{S0} site from the V_O. The d_{xz} –d_{yz} symmetry in figures 2(a) and (b) is the most stable solution (i.e., a d_{xz} orbital, rotated from the [001] towards the direction of the bonds with two equatorial bonds), but the polaron can be stabilized also with the $d_{x^2-y^2}$ (figures 2(c) and (d)) and d_{yz} (figures 2(e) and (f)) symmetries, with similar energy stability (ΔE = +25 and +40 meV with respect to the d_{xz}–d_{yz} solution, respectively). These different solutions can be spontaneously obtained by simply adopting different starting conditions in our DFT simulations, driving the system towards different minima of the energy configuration space. Polarons lying far from the vacancy, seem to adopt preferentially a d_{xz}–d_{yz} symmetry, while the nearest neighbor NN − Ti^A_{S0} site to the vacancy allows for the stabilization of a $d_{x^2-y^2}$ symmetry, but these localization sites are in general less favorable than the NNN − Ti^A_{S0} site [50, 65].

The stabilization of a different orbital symmetry can be attributed to surface effects and to the structural buckling of the TiO_2 surface structure: the tendency to stabilize the d_{xz}–d_{yz} symmetry is due to the misalignment between Ti^B_{S0} and Ti^A_{S0} atoms on the rutile surface that prevents the hybridization of the $d_{x^2-y^2}$ orbitals, typical for sub-surface polarons. However, surface oxygen vacancies perturb the local structure and partially suppress the buckling (see the distortions around the lattice defect in figures 1(a) and (e)): Ti^B_{S0} and Ti^A_{S0} atoms are practically aligned in the proximity of the V_O, and this alignment stabilizes a $d_{x^2-y^2}$ orbital symmetry for a polaron on the NN − Ti^A_{S0} or NNN − Ti^A_{S0} site, in analogy with the sub-surface Ti^A_{S1} polaron.

These different orbital symmetries can have different impact on the material properties: by considering for example the surface reactivity, the DFT calculations modeling the most favorable d_{xz} –d_{yz} symmetry well eproduce the ability of polarons to hybridize with CO adsorbates and form sta- ble complexes on the surface NNN –Ti^A_{S0} sites [54]. These complexes are characterized by peculiar double-lobe signals in scanning tunneling microscopy (STM) measurements, well reproduced by DFT; conversely, the polaron in $d_{x^2-y^2}$ orbital symmetry interacts less favorably with the CO molecule, showing a weaker hybridization and less intense single-spot in the simulated STM, not supported by the experiments [65].

Industrial Engineering Journal
ISSN: 0970-2555
Volume : 51, Issue 04, April : 2022

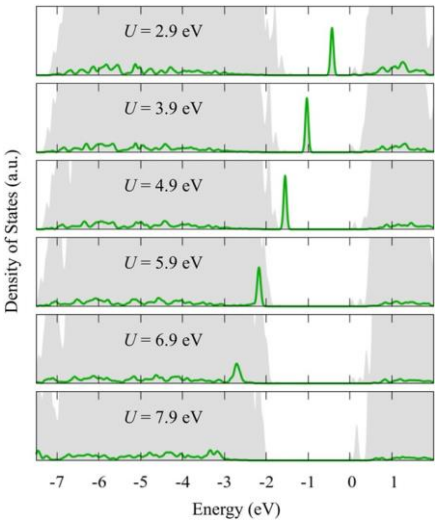

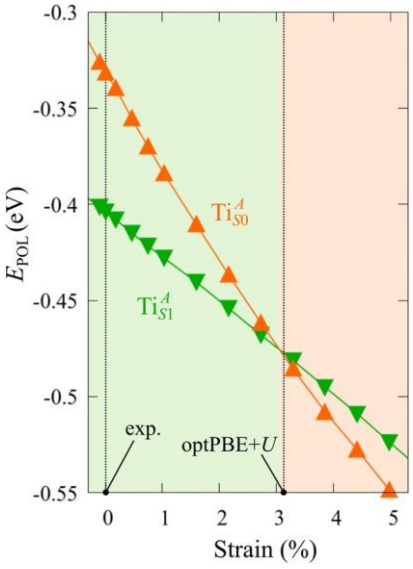

Figure 5. Effects of U on the polaronic state. The total DOS (filledgray) and the projection on the polaronic Ti^A atom (solid green line) are reported for various values of U (as indicated in every image).

NNN − Ti^A $_{S0}$ and Ti^A $_{S1}$ polarons (typically, the most favorable sites for polarons formation on the rutile surface). By using the cRPA U^{cRPA} value, Ti^A $_{S1}$ polarons are more favorable (by approximately 100 meV) than NNN Ti^A $_{S0}$ polarons. By adopting smaller U values, the polarons become less stable and eventually delocalize (the NNN − Ti^A $_{S0}$ polaron is destabilized already at U 3 while the Ti^A $_{S1}$ polaron is slightly more resistant). On the other hand, large U values favor the formation of NNN − Ti^A $_{S0}$ polarons: at approximately 1 eV above the U^{cRPA} value (U 5 eV) formation of Ti^A $_{S1}$ polarons becomes energetically less favorable than NNN Ti^A $_{S0}$. The crossing takes place at even lower U values for strongly reduced slabs (e.g., U 4.5 eV for c_{V_O} = 16.7%, not shown), closer to U^{cRPA}.

Considering that the stability of the $S0$ polarons is not typically supported by the experimental observations (on the clean surface, at low temperature), these large U values should be avoided in the calculations. Furthermore, the curves for both polarons show a kink at U 7 eV, with E_{POL} following a different linear trend at higher U values: this discontinuity can be understood by inspecting the corresponding electronicproperties, as discussed below.

The E_{POL} trend is associated to a modification of the polaronic in-gap state. Figure 5 shows the DOS obtained for the Ti^A_{S1} polaron. The position of the polaron state can be arbitrarily controlled by varying the U: upon variations of 1 eV around U^{cRPA} (up to approximately U = 5 eV), the polaron peak remains sharp and shifts within almost the whole energy gap. At higher U values, the polaronic state overlaps with the valence band, and, eventually, the d states of the hosting Ti site show no sharp features at U 4 7 eV, in correspondence with the discontinuity observed for E_{POL} (figure 4).

Figure 6. Effects of the lattice strain on the polaron stability. Formation energy E_{POL} for the NNN − Ti^A $_{S0}$ and Ti^A $_{S1}$ polarons (in a strongly reduced slab, c_{V_O} = 16.7%), as a function of the lattice strain along [001]. The dotted, vertical lines indicate the values for the [001] lattice vector as measured by the experiment and as obtained by slab relaxation at the optPBE +U level.

Lattice strain

The stability of small polarons depends on the strain applied to the crystal [66]. Polarons localized on Ti^A $_{S1}$ and NNN − Ti^A $_{S0}$ sites are characterized by different local lattice distortions, as discussed in the previous section: while the bond-length with the coordinated O atoms are elongated by both polarons, the Ti^A_{S1} polaron tends to attract the nearest-neighbor Ti atoms, while the NNN Ti^A $_{S0}$ repels the nearest Ti atoms. We can describe this scenario by considering the NNN Ti^A $_{S0}$ polaronas subjected to a compressive stress, while the Ti^A $_{S1}$ polaron experiences a tensile stress, as far as the surrounding Ti atoms are considered. This description suggests that these two inequivalent polarons could respond differently to strain. Figure 6 compares the effects of strain (applied along the [001] direction) on the energy stability E_{POL} for Ti^A $_{S1}$ and NNN − Ti^A $_{S0}$ polarons (with respect to the low-temperature experimental lattice constant c = 2.953 Å taken as reference, i.e., 0% strain [21]). As expected, a tensile strain along [001] enhances the stability of NNN Ti^A $_{S0}$ polarons to a larger extent as compared to the Ti^A $_{S1}$ polaron. Ultimately, for very large values of the strain (43%), a phase transition occurs: the NNN Ti^A $_{S0}$ sites become the most favorable sites for polaron formation. Even though the Ti^A $_{S1}$ atoms remain the most favorable hosting sites up to high amount of strain (≈3%), some spe-

Industrial Engineering Journal
ISSN: 0970-2555
Volume : 51, Issue 04, April : 2022

cific surface properties might get sensibly affected at smaller extent of strain, such as the surface reactivity (see discussion in the next section).

We conclude this section by underling the importance of the [001] lattice parameter used in the calculations to model the TiO_2(110) surface. Due to the known tendency of GGA-based DFT + U calculations to overestimate the unit cell volume, our optimized [001] lattice parameter is about 3% larger than the experimental one, biasing the relative stability between non-equivalent polarons. By using the low-temperature exper- imental parameters to model the system instead of relying on the calculated lattice, the results on the polaronic properties appear more reasonably in agreement with the experimental observation.

We note also that the calculated lattice parameter depends on the reduction level of the slab: larger concentrations of oxy-gen vacancies show a stronger elongation of the [001] vector (3.1% for c_{V_O} = 16.7%) as compared to the pristine surface (3.0%). This effect is probably due to the broken bonds on the surface at the V_O sites, and might explain the tendency of rutile sample to exhibit NNN $-$ Ti^A_{S0} polarons at highly reduc- ing conditions [51, 54]: the elongation along [001] mitigates the compressive stress on the NNN $-$ Ti^A_{S0} polaron, resulting in a stronger stability.

CO adsorption

Polarons play a decisive role for the surface reactivity of rutile TiO_2(110). The adsorption of CO molecules has been a well studied testbed case that has contributed to clarify the role of polarons in reaction processes [54, 67–74]. At low coverage, CO molecules adsorb in a vertical orientation on the TiO_2(110) surface. Adsorption on V_O sites is typically very favorable and not influenced by polarons. CO adsorption on the five fold coordinated Ti^A is instead driven by the polarons: at low CO coverage and highly reducing conditions, the molecules preferably adsorb at NNN Ti^A_{S0} sites, due to the coupling with NNN Ti^A -polarons, as recently reported by scan- ning probe experiments [54]. Weakly reduced samples exhibit few CO+NNN Ti^A -polaron complexes together with CO molecules adsorbing on sites at large distance from the V_O and from the Ti^A_{S1} polarons ($Ti^A_{S1} \leftrightarrow$ CO), showing no significant electronic coupling with the polaronic states.

Figure 7 shows the effects of strain on the properties of CO adsorption, as predicted by DFT calculations for a weakly reduced slab (c_{V_O} = 5.6%). As far as the low-temperature [001] lattice parameter is used in the simulations (0% of strain), DFT well describes the coexistence of CO+NNN Ti^A_{S0} -polaron complexes with $Ti^A_{S1} \leftrightarrow$ CO molecules (see the comparable E_{ads} values at 0% strain in figure 7) [54]. However, even modest tensile strain along [001] favors the polaron hopping towards the surface, and the CO+NNN Ti^A_{S0} -polaron com- plexes become dominant. Conversely, by applying strong com- pressive strain (-1%), the calculations predict a splitting of the CO+NNN Ti^A_{S0} -polaron complex, in favor of a polaron lying on a Ti^A_{S1} site below the CO molecule in the proximity of polaron complex, against experimental the V_O (labeled as CO@Ti^A_{S1} in the figure) in addition $Ti^A_{S1} \leftrightarrow$ CO configuration.

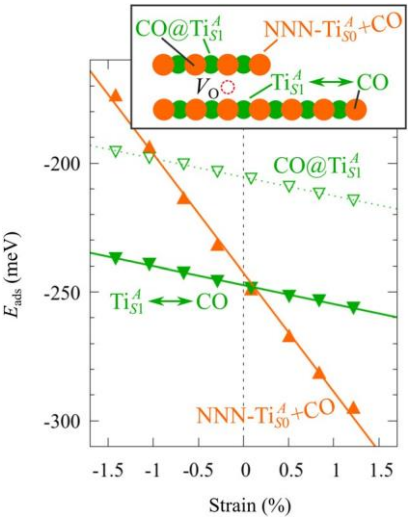

Figure 7. Tuning the adsorption process by applied strain. Adsorption energy E_{ads} for a CO molecule adsorbing at low reducing conditions (c_{V_O} = 5.6%), as a function of lattice strain applied along [001]. Three different adsorption configurations are considered: CO molecule adsorbing in the proximity of the V_O and coupling with a NNN Ti^A_{S0} polarons (orange, up-pointing triangles); CO molecule adsorbing in the proximity of the V_O above a sub-surface Ti^A_{S1} polaron (CO@Ti^A_{S1}, green, empty, down-pointing triangles); CO molecule adsorbing on a Ti site far from both the V_O and any Ti^A_{S1} polaron ($Ti^A_{S1} \leftrightarrow$ CO, green, filled, down-pointing triangles). The inset sketches the top view of the rutile surface, with the polaron localization and CO adsorption sites indicated by the labels (surface Ti atoms in orange circles, subsurface Ti atoms in smaller green circles).

Beside providing useful ways of controlling adsorption and catalysis processes, strain effects clearly indicate that calcula- tions performed using the DFT + U-optimized lattice constant overestimate unrealistically the stability of CO+NNN $-$ Ti^A_{S0} - observation. It is clear that comparison with experiment and accurate control over the polaron properties is crucial to obtain reasonable predictions.

4. Summary and conclusions

In summary, we reported a systematic DFT analysis on the properties of polarons on rutile TiO_2(110), focusing on the effects of lattice strain and computational details. The U parameter used in the calculation for correcting the electronic correlation on transition metals shows a broad impact, influ- encing the charge localization, the local lattice distortions and the electronic state of the polarons. Different types of polarons

ing on the adopted parameter: the sub-surface polarons typically reported by the experiments are predicted as the most stable type for U values ranging ± 1 eV around the $U^{\mathrm{cRPA}} = 3.9$ eV value calculated by cRPA simulations in the bulk. Moreover, charge trapping can be driven to different lattice sites upon applied strain: this suggests a possible mechanism for controlling the polaron localization, in addition to underline the importance of a careful parametrization in the calculations. The modeling of the excess electrons is indeed a delicate task, due to a potential energy surface characterized by numerous local minima [75], determined by the various possible polaron arrangements and the different electronic properties of these electronic states. The benchmark with experiments is of fundamental importance in order to obtain reliable predictions [76, 77] and to accurately describe complex phenomenainfluenced by polarons [1].

Additionally, we showed how the functionalities of polaronic materials can be tuned by controlling the polaron properties. We focused on the adsorption of CO molecules: CO adsorbates can be driven to different adsorption sites upon application of strain, arbitrarily favoring or disfavoring the coupling with surface polarons. Control over the adsorption process and the electronic properties of the adsorbates represent an interesting and coveted feature that could be exploited for applications in the field of catalysis.

Finally, we note that the development of efficient functional oxide materials requires an accurate atomic-scale understanding of the effects brought about by oxidation and reduction reactions. Our study highlights the importance of a precise modeling of reducible oxides and the need to account for different arrangement and types of polarons, which can be achieved by extensive exploration of the polaronic configuration space [27, 35, 51, 78, 79].

References

[1] Franchini C, Reticcioli M, Setvin M and Diebold U 2021 *Nat. Rev. Mater.* **6** 560
[2] Sugawara E and Nikaido H 2014 *Antimicrob. Agents Chemother.* **58** 7250
[3] Landau L D and Pekar S I 1965 *Collected Papers of L D Landau* vol 53 (Elsevier) pp 478–83
[4] Fröhlich H, Pelzer H and Zienau S 1950 *London, Edinburgh Dublin Phil. Mag. J. Sci.* **41** 221
[5] Holstein T 1959 *Ann. Phys., NY* **8** 325
[6] Emin D 2013 *Polarons* (Cambridge: Cambridge University Press)
[7] Alexandrov A S and Devreese J T 2010 *Advances in Polaron Physics* (*Springer Series in Solid-State Sciences*) vol 159 (Berlin: Springer) p 171
[8] Jupille J and Thornton G 2015 *Defects at Oxide Surfaces* (*Springer Series in Surface Sciences*) vol 58 ed J Jupille and G Thornton (Cham: Springer International Publishing) pp 327–49
[9] Austin I G and Mott N F 2001 *Adv. Phys.* **50** 757
[10] Stoneham A M, Gavartin J, Shluger A L, Kimmel A V, Ramo D M, Rønnow H M, Aeppli G and Renner C 2007 *J. Phys.: Condens. Matter* **19** 255208
[11] Ghosh D, Welch E, Neukirch A J, Zakhidov A and Tretiak S 2020 *J. Phys. Chem. Lett.* **11** 3271
[12] Zhugayevych A and Tretiak S 2015 *Annu. Rev. Phys. Chem.* **66** 305
[13] Haneef H F, Zeidell A M and Jurchescu O D 2020 *J. Mater. Chem.* C **8** 759
[14] Wu L, Fu C and Huang W 2020 *Phys. Chem. Chem. Phys.* **22** 9875
[15] Pelli Cresi J S, Di Mario L, Catone D, Martelli F, Paladini A, Turchini S, D'Addato S, Luches P and O'Keeffe P 2020 *J. Phys. Chem. Lett.* **11** 5686
[16] Rousseau R, Glezakou V-A and Selloni A 2020 *Nat. Rev. Mater.* **5** 460
[17] Dohnálek Z, Lyubinetsky I and Rousseau R 2010 *Prog. Surf. Sci.* **85** 161
[18] Yim C M *et al* 2018 *J. Phys. Chem. Lett.* **9** 4865
[19] Yin W-J, Wen B, Zhou C, Selloni A and Liu L-M 2018 *Surf. Sci. Rep.* **73** 58
[20] Liu B, Zhao X, Yu J, Parkin I P, Fujishima A and Nakata K 2019 *J. Photochem. Photobiol.* C **39** 1–57
[21] Diebold U 2003 *Surf. Sci. Rep.* **48** 53
[22] Bogomolov V N and Mirlin D N 1968 *Phys. Status Solidi b* **27** 443
[23] Dominik L A K and MacCrone R K 1967 *Phys. Rev.* **156** 910
[24] Bredow T and Pacchioni G 2002 *Chem. Phys. Lett.* **355** 417
[25] Di Valentin C, Pacchioni G and Selloni A 2006 *Phys. Rev. Lett.* **97** 166803
[26] Di Valentin C, Pacchioni G and Selloni A 2009 *J. Phys. Chem.* C **113** 20543
[27] Pham T D and Deskins N A 2020 *J. Chem. Theory Comput.* **16** 5264
[28] Di Valentin C, Finazzi E, Pacchioni G, Selloni A, Livraghi S, Czoska A M, Paganini M C and Giamello E 2008 *Chem. Mater.* **20** 3706
[29] Deskins N A, Rousseau R and Dupuis M 2009 *J. Phys. Chem.* C **113** 14583
[30] Janotti A, Varley J B, Rinke P, Umezawa N, Kresse G and Van De Walle C G 2010 *Phys. Rev.* B **81** 085212
[31] Deák P, Aradi B and Frauenheim T 2012 *Phys. Rev.* B **86** 195206
[32] Kullgren J, Huy H A, Aradi B, Frauenheim T and Deák P 2014 *Phys. Status Solidi* **8** 566
[33] Moses P G, Janotti A, Franchini C, Kresse G and Van De Walle C G 2016 *J. Appl. Phys.* **119** 181503
[34] Reticcioli M, Diebold U, Kresse G and Franchini C 2020 *Handbook of Materials Modeling* (Cham: Springer International Publishing) pp 1–39
[35] Setvin M, Franchini C, Hao X, Schmid M, Janotti A, Kaltak M, Van De Walle C G, Kresse G and Diebold U 2014 *Phys. Rev. Lett.* **113** 086402
[36] Li J, Chenot S, Jupille J and Lazzari R 2021 *J. Phys. Chem.* C **125** 16652
[37] Tanner A J, Wen B, Ontaneda J, Zhang Y, Grau-Crespo R, Fielding H H, Selloni A and Thornton G 2021 *J. Phys. Chem. Lett.* **12** 3571
[38] Tanner A J and Thornton G 2022 *J. Phys. Chem. Lett.* **13** 559
[39] De Lile J R, Bahadoran A, Zhou S and Zhang J 2021 *Adv. Theory Simul.* **5** 2100244
[40] Dudarev S L, Botton G A, Savrasov S Y, Humphreys C J and

Sutton A P 1998 *Phys. Rev.* B **57** 1505
[41] Lany S and Zunger A 2009 *Phys. Rev.* B **80** 085202
[42] Lany S 2011 *Phys. Status Solidi b* **248** 1052
[43] Spreafico C and VandeVondele J 2014 *Phys. Chem. Chem. Phys.* **16** 26144
[44] Kokott S, Levchenko S V, Rinke P and Scheffler M 2018 *New J. Phys.* **20** 033023
[45] Farzalipour Tabriz M, Aradi B, Frauenheim T and Deák P 2017 *J. Phys.: Condens. Matter* **29** 394001
[46] Elmaslmane A R, Watkins M B and McKenna K P 2018 *J. Chem. Theory Comput.* **14** 3740
[47] Deskins N A, Rousseau R and Dupuis M 2011 *J. Phys. Chem.* C **115** 7562